Raman spectroscopy on carbon nanotubes at high pressure

I. Loa
Max-Planck-Institut für Festkörperforschung, D-70569 Stuttgart, Germany

arXiv:cond-mat/0307356v1 15 Jul 2003

Abstract

Raman spectroscopy has been the most extensively employed method to study carbon nanotubes at high pressures. This review covers reversible pressure-induced changes of the lattice dynamics and structure of single- and multi-wall carbon nanotubes as well as irreversible transformations induced by high pressures. The interplay of covalent and van-der-Waals bonding in single-wall nanotube bundles and a structural distortion near 2 GPa are discussed in detail. Attempts of transforming carbon nanotubes into diamond and other "superhard" phases are reviewed critically.

Keywords: carbon nanotubes, Raman spectroscopy, high pressure, lattice dynamics, phase transition.

Ingo Loa
Max-Planck-Institut für Festkörperforschung
Heisenbergstr. 1
D-70569 Stuttgart
Germany

phone +49.711.689–1469; fax –1444
E-mail: I.Loa@fkf.mpg.de

To appear in J. Raman Spectroscopy (July/August 2003): Special Issue on »Extreme Conditions«.

Contents

1 Introduction **3**

2 Background **4**

2.1 Basic Properties of Carbon Nanotubes 4

2.2 Synthesis of Carbon Nanotubes 5

3 Lattice Dynamics and Structure of SWNTs **7**

3.1 Radial Breathing Mode 7

3.2 Tangential Modes 11

3.3 Anomaly at 2 GPa 15

4 Lattice Dynamics of MWNTs **20**

5 Structural Transformations of Carbon Nanotubes **22**

6 Concluding Remarks **29**

7 Acknowledgements **29**

1 Introduction

Single-wall carbon nanotubes (SWNTs) are tubular macromolecules with typical diameters on the order of 1 nm and lengths up to several µm that are made purely from carbon. As a consequence of their small diameter and very large length-to-diameter ratio, *isolated* nanotubes represent nearly ideal realizations of a one-dimensional system, in particular with regard to their electronic properties. Solid SWNT material produced by the common growth techniques, however, usually consists of tangled bundles containing up to a few hundred aligned nanotubes. Mechanically, carbon nanotubes combine high stiffness and tensile strength with low density. Their fascinating structure and special characteristics as well as the prospect of numerous technical applications has led to intense research on this material over the last decade. Part of the potential applications [1] – including electron field emission [2], field-emission displays [3, 4], hydrogen storage [5], single electron transistors [6], gas sensors [7], and nanomechanical devices [8] – have been realized during recent years. The discovery of the single-wall carbon nanotubes in 1993 [9, 10] was preceded by the observation of multi-wall nanotubes (MWNTs) two years earlier [11]. The latter consist of a coaxial series of carbon tubes nested one inside the other.

Application of high pressures is the ideal tool to tune continuously the bonding properties of a solid. The structural variations affect virtually all material properties. In the context of carbon nanotubes, the pressure-induced changes of the vibrational characteristics are of particular interest. They yield, although indirectly, important information on the bonding properties, especially with regard to the interplay of covalent and van-der-Waals (vdW) bonding. In addition, structural transformations manifest themselves in changes of the lattice dynamics. The vibrational properties of nanotubes in a high-pressure diamond anvil cell (DAC) can readily be investigated by Raman spectroscopy which has played an important role in the field of carbon nanotubes for a long time.

This review is organized as follows. Section 2 summarizes some basic background information on the properties and synthesis of carbon nanotubes. Reversible pressure-induced changes of the lattice dynamics and structure of single-wall and multi-wall nanotubes will be discussed in sections 3 and 4, respectively. Section 5 addresses the question of irreversible pressure-induced structural transformations, especially towards hard phases such as diamond. Finally, perspectives on possible future developments are briefly presented in the concluding section 6.

2 Background

Comprehensive treatments of the synthesis, characterization, properties and applications of carbon nanotubes were presented in several books and review articles, see e. g. Refs. [12, 13, 14, 15]. Here, we shall summarize briefly some basic information to make this short review reasonably self-contained.

2.1 Basic Properties of Carbon Nanotubes

Single-wall carbon nanotubes can be thought of as being formed by rolling a graphene sheet into a cylinder (Fig. 1). Depending on how the sides of the sheets are joined, nanotubes of different diameter and helicity are obtained. All possible structures are uniquely identified by a pair of integer numbers, the *roll-up vector* (n, m). It defines the chirality vector $\boldsymbol{C}_h = n\boldsymbol{a}_1 + m\boldsymbol{a}_2$ that connects two symmetry-equivalent atoms of the 2D graphene sheet (Fig. 1). After rolling the graphene sheet into a tube, the chiral vector becomes a circumferential line of the tube. SWNTs with a roll-up vector of the form $(n, 0)$ are called *zigzag* tubes. *Armchair* tubes are characterized by a roll-up vector (n, n). Both types are *achiral* tubes; all other tubes are referred to as *chiral* nanotubes. The diameter of a carbon nanotube is given by

$$d_{nm} = |\boldsymbol{C}_h|/\pi = \sqrt{3}a_{\mathrm{C\text{–}C}}(m^2 + nm + n^2)^{1/2}/\pi, \tag{1}$$

where $a_{\mathrm{C\text{–}C}}$ denotes the carbon–carbon bond length (1.42 Å). Single-wall nanotubes grown by the common arc-discharge or laser-ablation methods [13, 16] usually exhibit a narrow distribution of diameters. A typical average diameter of 1.4 nm is close to that of a $(10, 10)$ nanotube. SWNTs do not generally exist as individual tubes. They rather form bundles of up to a few hundred tubes in a regular hexagonal lattice [17, 9, 10].

The electronic properties of SWNTs depend on their structure. There are metallic, semimetallic, and semiconducting SWNTs with electronic band gaps up to ∼1 eV. Being derived from graphene sheets, carbon nanotubes show predominantly sp^2-type bonding of the carbon atoms. Deviation from the planar bonding introduces, however, some sp^3-type hybridization. In view of the strong covalent bonding, carbon nanotubes have been expected to exhibit high stiffness and tensile strength. Measurements of mechanical quantities are difficult to perform on individual tubes. Nonetheless, such experiments were carried out and large values of Young's modulus on the order of 1 TPa were reported [18, 19, 20].

Raman spectroscopy has become a widespread tool for the investigation as well as the routine characterization of carbon nanotubes [13]. It yields information on the vibrational and, indirectly, on the structural properties. Raman spectra of SWNTs typically show intense peaks in the spectral ranges of 160–200 and 1500–1600 cm^{-1}(Fig. 2). The first assignment of these features was given by Rao *et al.* [21]. The low-energy peaks are attributed to a *radial breathing mode* (R band), where all C atoms are subject to an in-phase radial displacement. This mode is rather strongly diameter-dependent and was therefore proposed as a means to determine the SWNT diameter [22]. The higher-energy peaks are attributed to modes with neighboring C atoms vibrating out-of-phase parallel to the surface of the cylinder (*tangential modes*, T band) [21] which are related to the $E_{2g}(2)$ phonon at ∼1580 cm^{-1} in graphite [23, 24, 25, 26]. In achiral tubes, one can distinguish two tangential modes with atomic displacements parallel and perpendicular to the tube axis, respectively. Besides these Raman-active vibrations, there exists a defect-related

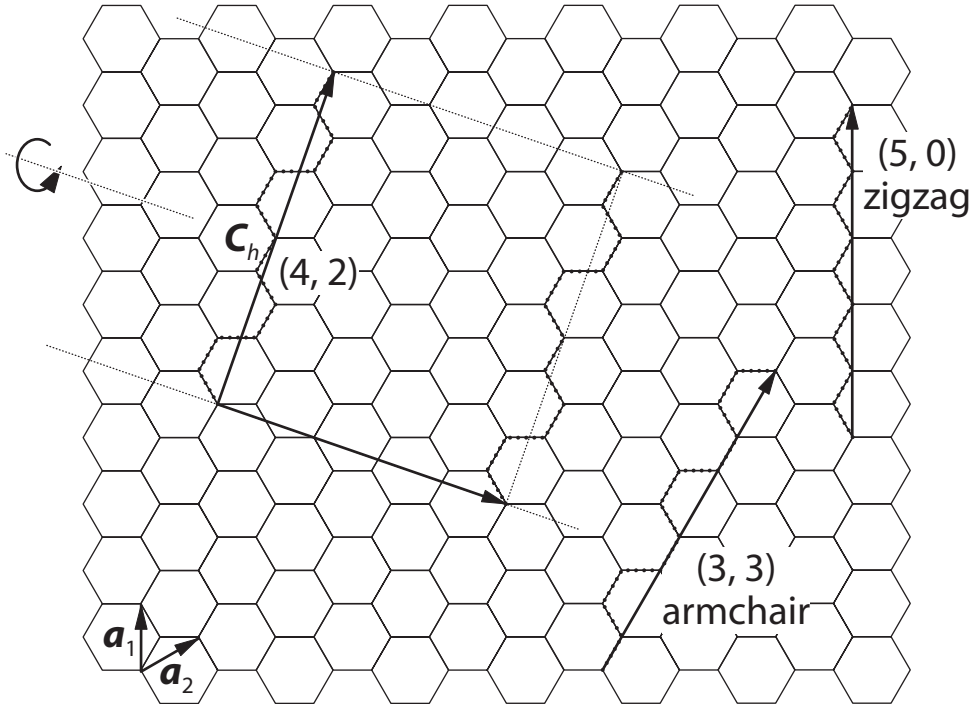

Figure 1: Rolling-up of a graphene sheet into a nanotube. The geometry of a single-wall nanotube is defined by the roll-up vector (n, m) or, equivalently, the chiral vector $\boldsymbol{C}_h = n\boldsymbol{a}_1 + m\boldsymbol{a}_2$. The chiral vectors of a zigzag and an armchair tube are also shown.

mode near 1350 cm^{-1} that is known from graphite [27]. Overtone and combination modes of the above excitations have also been observed.

Multi-wall carbon nanotubes usually consist of several tens of concentric shells. The spacing between the sheets equals approximately the interlayer distance in graphite (3.4 Å). Like in the case of the SWNTs, bending of the graphene sheets has little influence of the structural and electronic properties. This applies all the more to MWNTs because of their larger diameter, i. e., smaller curvature of the layers. Besides the geometry, the most important difference between MWNTs and graphite is the confinement of the charge carriers to the tubular structure of the nanotubes. Many physical properties of MWNTs are quite similar to those of graphite.

2.2 Synthesis of Carbon Nanotubes

Until recently, two methods have dominated the production of carbon nanotubes: *arc-discharge* (AD) growth and synthesis by *pulsed-laser vaporation* (PLV) [28, 10, 17, 16]. Both methods are based on the evaporation of carbon from a solid source. In the arc-discharge method, a He plasma is created between two opposing carbon electrodes. Carbon is evaporated at temperatures of 3000–4000 K. It condenses at lower-temperature areas of the cathode and forms nanotubes and other carbon particles, depending on the growth conditions. For the growth of SWNTs yttrium and/or transition metals need to be used as a catalyst. A typical mixture for the anode contains 1 at. % of Y and 4.2 at. % of Ni besides the carbon (graphite) [29]. In the PLV process, evaporation of carbon is achieved by laser ablation from a carbon target in a furnace at ∼1500 K [17]. The characteristics, in particular the diameter distribution and the yield of the

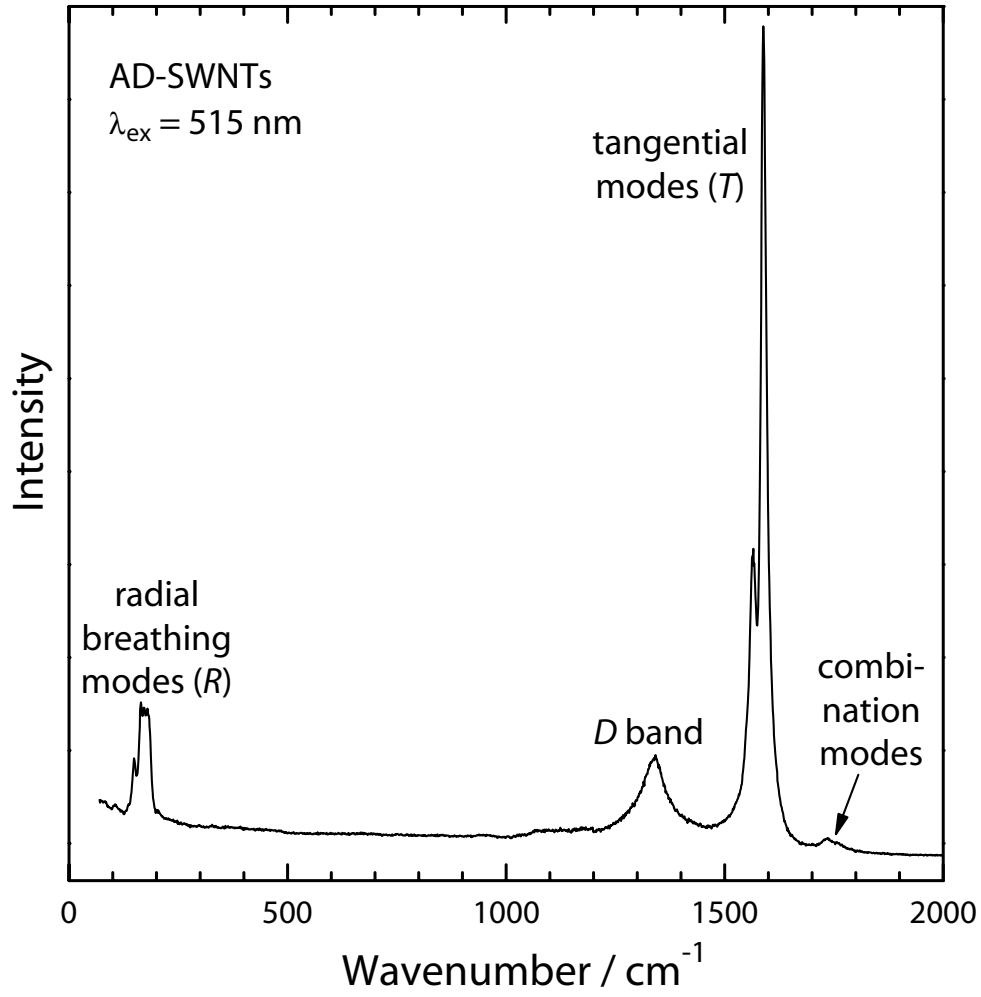

Figure 2: Raman spectrum of arc-discharge-grown SWNTs at ambient conditions ($\lambda_{\text{ex}} = 515$ nm).

nanotubes can be controlled by the choice of catalysts and growth conditions (inert gas pressure, discharge current, ...).

Removal of the metal catalyst particles and by-products such as fullerenes, graphitic polyhedrons, and amorphous carbon can be achieved by a purification process. It involves refluxing the as-grown material in a nitric acid solution, resuspending the nanotubes in pH-10 water with a surfactant, and filtration [30], possibly followed by a heat-treatment in vacuum to remove residues of the chemical treatment. This method produces a free-standing mat of tangled SWNT ropes, so-called *bucky paper*.

As an alternative, chemical vapor deposition (CVD) has been employed for the growth of carbon nanotubes [16]. It had been used for the production of carbon fibers and filaments before the advent of carbon nanotubes. While it has been challenging to produce structurally perfect nanotubes by this method, it offers the possibility to grow ordered and aligned nanotube structures [31, 16]. Furthermore, nanotube growth at specific locations on a surface can be achieved by employing contact printing or lithographic techniques to control the deposition of the catalyst on a substrate [16].

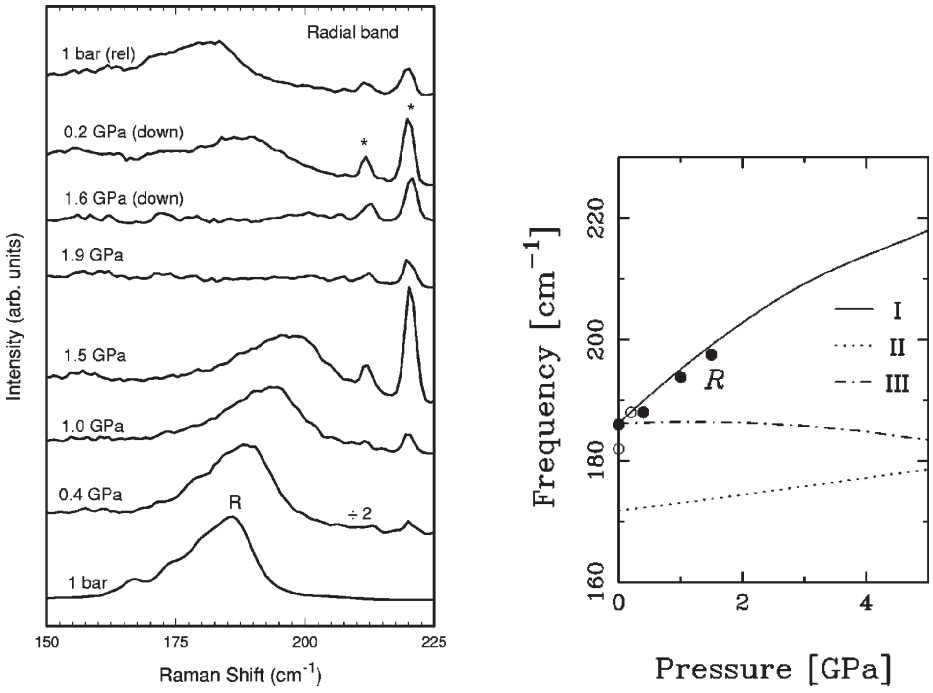

Figure 3: (left) Raman spectra of PLV-SWNT bundles in the region of the radial breathing mode as a function of pressure ($T = 300$ K, excitation wavelength $\lambda_{ex} = 515$ nm). The R band disappears beyond 1.5 GPa. (right) Pressure dependence of the radial mode wavenumber. Solid (open) symbols refer to data measured during the upward (downward) cycle of pressure. The lines show results of GTBMD calculations (models I–III in Ref. [32]) for a $(9, 9)$ nanotube bundle. Reproduced from Ref. [32].

3 Lattice Dynamics and Structure of SWNTs

The vibrational properties of single-wall carbon nanotubes under hydrostatic pressure have been investigated in numerous Raman scattering studies. In the following two sections, results on the radial mode and the tangential modes will be reviewed, respectively. In either case, there are indications of a structural distortion or transition near 2 GPa that will discussed in section 3.3.

3.1 Radial Breathing Mode

Basic Results The first study of the effect of hydrostatic pressure on the Raman spectrum of SWNTs was published by Venkateswaran *et al.* [32]. Figure 3 shows Raman spectra of as-prepared PLV-SWNT bundles in the spectral region of the R band [32]. The common 4:1 methanol/ethanol mixture was used as the pressure transmitting medium in the diamond anvil cell. The R band shifts towards higher wavenumbers with increasing pressure at rate of 7 ± 1 cm^{-1}/GPa. The R band decreases in intensity as the pressure is increased, and it vanishes beyond 1.5 GPa in contrast to the higher-energy tangential modes (section 3.2). Upon pressure reduction from 5.2 GPa, the R band reappears around 1.5 GPa. After the pressure cycle, the R mode recovered only part of its initial intensity.

In place of the common methanol/ethanol pressure medium, Obratzsova *et al.* [33] used condensed nitrogen as a pressure transmitter, that is fluid up to 2.5 GPa (at ambient temperature)

Table 1: Compilation of Raman scattering and theoretical results on carbon nanotube phonon wavenumbers ω_0 and their respective pressure dependences $\mathrm{d}\omega/\mathrm{d}P$. The experimental T-band data refer to the most intense component of the T-band. Grouped together are experiments that appear to have been performed on samples of the same origin. A 4:1 methanol/ethanol mixture (M/E) was used as a pressure medium, unless noted otherwise (H_2O, N_2, He, M/E/W {16:3:1 methanol/ethanol/water}).

	R-band		T-band					
sample	ω_0 (cm^{-1})	$\mathrm{d}\omega/\mathrm{d}P$ (cm^{-1}/GPa)	ω_0 (cm^{-1})	$\mathrm{d}\omega/\mathrm{d}P$ (cm^{-1}/GPa)	P range (GPa)	λ_{ex} (nm)	reference	notes
experiment								
PLV SWNT (1)	186	7(1)	1593(1)	∼4.9[a]	0–5.5	515	[32, 40]	
				7.5	0–2			
				4.8	2–5.5			
PLV SWNT (2)	181(3)	10.1(12)	1591	10.1(11)	0–1.7	515	[34]	
				5.8(2)	1.7–5.3			
PLV bucky paper	186	∼10	1592	4.9	0–10	488	[33, 41]	N_2
PLV s-SWNT	190	8.4	?	∼5.1[d]	0–4.8	515	[40, 42]	
				7.8	0–1.8			
				4.7	1.8–4.8			
AD SWNT	171	9.7(5)	1593	5.7	0–10	515	[35, 36]	
			1592	6.0	0–10	647	[43]	
AD bucky paper (1)	172	9.6	1595	5.3	0–10	515	[37, 38]	M/E/W
				4.5	16–25			M/E/W
			1594	6.1	0–10		[39]	M/E/W
			1596	7.1	0–7			H_2O
	170	9.1						M/E/W & H_2O
	180	8.1						M/E/W & H_2O
AD bucky paper (2)	173	8.3(1)	1598(1)	5.8(1)	0–9	515	[40]	
MWNT (1)			1583	4.3	0–10	515	[36]	
MWNT (2)			1583(1)	3.8(1)	0–9	515	[40]	M/E
				3.7(1)	1–9			He
graphite			1579	4.7			[25]	
theory								
(9, 9) bundle	186.2	∼8.3[b]	1576	∼6.6[c]	0–5.5		[32]	model I
(10, 10) bundle	162	14	1690	11	0.1–0.5		[44]	

[a] linear approximation to the relation $\omega(P) = \omega_0 + aP + bP^2$ with $a = 7.1(8)$ and $b = -0.4(2)$ given in the original work
[b] linear approximation [$a = 9.6,\ b = -0.65$]
[c] linear approximation [$a = 8.3,\ b = -0.31$]
[d] linear approximation [$a = 7.0,\ b = -0.35$]

and provides quasi-hydrostatic conditions to several tens of GPa. Here, the R band of PLV bucky paper was observed to shift at a rate of ∼10 cm^{-1}/GPa. This is larger than the shift observed by Venkateswaran *et al.* [32], but consistent with results of Peters *et al.* [34], Thomsen *et al.* [35,36], and Sood *et al.* [37,38]. Teredesai *et al.* [39] employed water as a pressure medium, that solidifies near 1 GPa (at 300 K), and found for the R band essentially the same pressure dependence as in the case of a 16:3:1 mixture of methanol/ethanol/water. Altogether, pressure shifts of the R band wavenumber in the range 7–10 cm^{-1}/GPa have been reported, with no clear correlation between the shift rate and the sample type or experimental conditions. Table 1 summarizes the numerical results of all the studies cited here and in the next section.

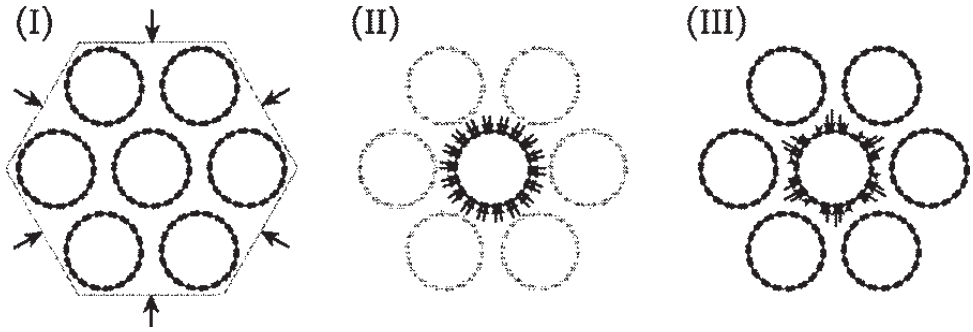

Figure 4: Cross-sectional view of a SWNT bundle showing schematically the forces on the bundle and the individual tubes in the triangular lattice when hydrostatic pressure is applied. In model I, the entire bundle is subjected to an external compression. In model II, the individual tubes are each compressed symmetrically, and intertubule coupling is ignored. The absence of vdW interactions between the tubes is shown schematically by the lightly shaded tubes surrounding the center tube. In model III, the pressure medium is allowed to penetrate into the interstitial channels between tubes and thereby exerts a $\sin^2 3\Theta$ force on the tubes. Models I and III include intertubule vdW coupling. Reproduced from Ref. [32].

Lattice Dynamical Calculations To aid the interpretation of their experimental results, Venkateswaran *et al.* [32] performed calculations of the radial and tangential modes frequencies of a $(9,9)$ SWNT bundle, using a generalized tight-binding molecular dynamics (GTBMD) scheme. Going beyond the original formulation of this method [45], they treated the van-der-Waals-type (vdW) intertubule interaction by the addition of a Lenard-Jones-type potential to the GTBMD. Three models of the interaction of the pressure medium with the nanotube bundles were considered as shown in Fig. 4. Comparison of the theoretical and experimental results in Fig. 3 shows that only their model I, where the pressure medium does not penetrate the bundles, is in agreement with the experiment. Comparison between model I and model II (without vdW forces) demonstrates the importance of the initially weak intertubule interaction for the experimentally observed pressure dependence of the radial mode frequency. None of the pressure media alcohol, water, and nitrogen that have been employed in the various studies appears to penetrate into the interstitial channels (diameter $\sim$2.6 Å [32]) between the bundled carbon nanotubes.

Intertubule Interaction It was noticed [32] that inclusion of the intertubule vdW interaction in the calculation leads to an up-shift of the zero-pressure R mode wavenumber by $\sim$14 cm^{-1} ($\sim$8%). Further tight-binding calculations by Kahn and Lu [44] as well as Henrard *et al.* [46,47] predicted a 6–24 cm^{-1} increase in wavenumber for the R modes in bundled nanotubes with diameters of 10–16 Å compared to those of the respective isolated tubes. These are important results as the R mode wavenumber ω_R was proposed [22, 48] as a measure for the nanotube diameter d_t (Eq. 1) via the relation $\omega_R = 223.75(\text{cm}^{-1} \times \text{nm})/d_t$. If one neglects the small dependence [47] of the vdW-related wavenumber shift on nanotube geometry for the range of tube diameters of experimental interest, this leads to a modified relation between R mode wavenumber and tube diameter, $\omega_R \approx 224(\text{cm}^{-1} \times \text{nm})/d_t + \Delta_{\text{vdW}}$, where Δ_{vdW} is on the order of 15 cm^{-1}. However, recent experiments [49] on very small bundles containing only a few nanotubes, so-called solubilized tubes (s-SWNT [50,51]), have evidenced a small up-shift of the R mode Raman peak

in the *debundled* tubes compared to the bundled ones. The apparent contradiction to the above lattice dynamical predictions was resolved by also taking into account the effect of intertube interaction on the electronic density of states as well as the known diameter-selective resonance effects in the Raman scattering process [21,52,53]. Altogether, the intertube interaction has been estimated to lead to a down-shift of the R mode *Raman peak* of $\sim$4 cm^{-1} for metallic tubes and $\sim$40 cm^{-1} for semiconducting tubes, despite the up-shift of the R mode *vibrational frequency* on the order of 15 cm^{-1}. It is unclear at present to what extent the pressure-induced changes of the electronic structure affect the shift of the R mode Raman peak under pressure.

The effect of intertubule interaction was further studied by Schlecht *et al.* [40, 42] in a high-pressure experiment on the above-mentioned solubilized nanotubes. From a height-profile analysis of scanning force microscopy images [50, 51], these s-SWNTs were deduced to contain nanotubes mostly in small bundles of 3–7 tubes, but also some isolated tubes. Although the ambient-pressure R mode energy is affected by the reduction in bundle size [49], they observed, surprisingly, a shift rate of 8.4 cm^{-1}/GPa which equals the average value for the R band in bundled SWNTs. At this stage it appears as if the vdW interaction with as few as two neighboring nanotubes in a bundle were sufficient to induce the large pressure shift observed in bundled SWNTs and attributed to the intertube interaction.

Elasticity Theory The normalized pressure dependence $\omega_0^{-1}\mathrm{d}\omega/\mathrm{d}P \equiv \mathrm{d}\ln\omega/\mathrm{d}P$ of the radial mode is larger by a factor of $\sim$15 than that of the tangential modes (section 3.2) or graphite [25]. The importance of the vdW forces between the tubes was illustrated by Thomsen *et al.* [35] in the framework of elasticity theory. Here, a nanotube is approximated by a hollow cylinder with isotropic elastic properties within the sheet that is rolled up [54, 36, 55]. Under hydrostatic pressure, the ratio of the circumferential to axial strain was deduced as $u_{\Theta\Theta}/u_{zz} = 1.9$. The assumption of similar dependences on strain, rather than pressure, for the radial and tangential modes, led Thomsen *et al.* to the expectation that the logarithmic pressure dependence of the R mode should only be about twice as large as that of the tangential modes in the absence of the vdW forces. Assuming additive force constants, the logarithmic pressure dependence of the R mode in a bundle can be separated into a contribution $(1-\alpha)$ from the radial breathing mode of the isolated tube (ω_{RBM}) and a contribution α from the van-der-Waals interaction (ω_{vdW}),

$$\frac{\mathrm{d}\ln\omega}{\mathrm{d}P} = \left(\frac{\omega_{\mathrm{RBM}}}{\omega_0}\right)^2 \frac{\mathrm{d}\ln\omega_{\mathrm{RBM}}}{\mathrm{d}P} + \left(\frac{\omega_{\mathrm{vdW}}}{\omega_0}\right)^2 \frac{\mathrm{d}\ln\omega_{\mathrm{vdW}}}{\mathrm{d}P} \tag{2}$$

$$= (1-\alpha)\frac{\mathrm{d}\ln\omega_{\mathrm{RBM}}}{\mathrm{d}P} + \alpha\frac{\mathrm{d}\ln\omega_{\mathrm{vdW}}}{\mathrm{d}P} \quad . \tag{3}$$

Taking the pressure derivative of the RBM term to be that of the intramolecular high-energy graphite mode (0.003 GPa^{-1} [25]) and the van-der-Waals component to correspond to the pure van-der-Waals type B_{1g} mode of graphite (0.15 GPa^{-1} [56]), led to the conclusion that the force constant of the R mode is to $\alpha = 37\%$ of van-der-Waals nature. This is equivalent to an up-shift of the radial breathing mode from 136 cm^{-1} for an isolated tube to 171 cm^{-1} in a bundle. Although the van-der-Waals contribution is somewhat overestimated in comparison to the tight-binding results, it demonstrates its importance and illustrates how mechanical properties of *mesoscopic* carbon nanotubes can be studied with the relatively simple continuum mechanical model [55].

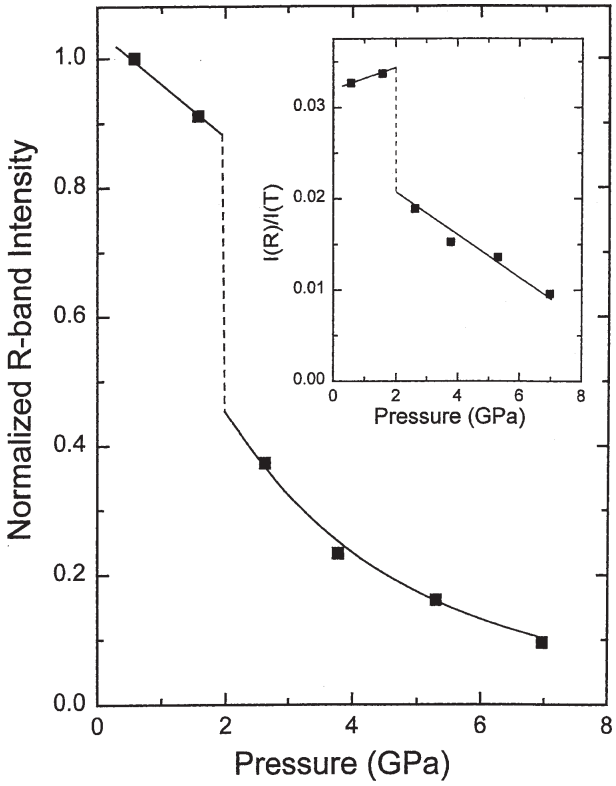

Figure 5: R band integrated intensity of AD-SWNT bucky paper as a function of pressure, normalized to its value at 0.5 GPa (λ_{ex} = 515 nm). The lines are guides to the eye. The inset shows the ratio of the R band to T band integrated intensity. The abrupt discontinuity near 2 GPa is apparent in the insert since the discontinuity in the T band intensity is not as pronounced as that of the R band. Reproduced from Ref. [40].

***R*-Mode Disappearance** Reduction in intensity and broadening of the R-mode Raman peak with increasing pressure as well as its disappearance near 2 GPa have been confirmed in a number of investigations with excitation at 515 nm [35,38,34] and 488 nm [33]. In one experiment on arc-discharge SWNT bucky paper [40], the R mode could be followed up to 7 GPa, but a discontinuous drop in intensity was observed near 2 GPa (Fig. 5). The intensity decrease under pressure was tentatively attributed to a loss in the electronic resonance of the Raman scattering cross section due to a hexagonal distortion in the cylindrical cross section of the nanotubes in bundles under compression [32]. Further experimental results on the tangential modes under pressure indicate a subtle structural transition near 2 GPa that will be discussed in detail in section 3.3.

3.2 Tangential Modes

Basic Results Figure 6 shows Raman spectra of as-prepared AD-SWNT bundles [36]. In the region of the T band, the Raman spectra exhibit three components, all of which shift towards higher wavenumbers with increasing pressure (Fig. 7). In this experiment, all components of the T band exhibited essentially the same pressure dependence of 5.7–5.8 cm^{-1}/GPa. Other experiments [37,38,40,39,43] on AD SWNTs employing methanol/ethanol as a pressure medium give similar results, i.e., wavenumber shifts of 5.3–6.1 cm^{-1}/GPa for the most intense component

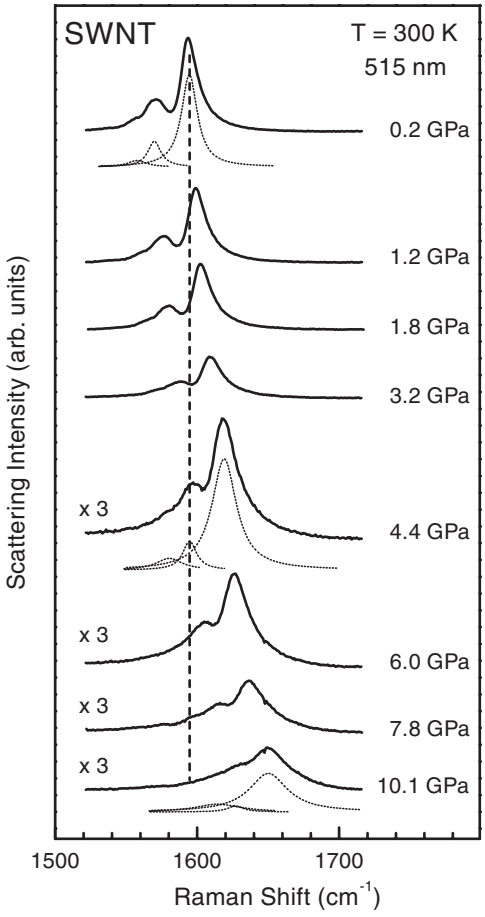

Figure 6: Raman spectra in the tangential-mode region of arc-discharge grown SWNTs for increasing hydrostatic pressures up to 10 GPa. Solid lines represent the experimental data and dotted ones the decomposition of the spectra into three peaks. Reproduced from Ref. [36].

of the T band (Table 1). In PLV-grown samples, the average pressure-induced shifts appear to be somewhat smaller. All of the studies on PLV samples [32, 40, 33, 42] except for that by Peters *et al.* [34] report wavenumber shifts of 4.7–5.1 cm^{-1}/GPa. The difference between AD- and PLV-grown samples may be related to the smaller average diameter of the latter. The phonon-frequency calculations by Kahn and Lu [44] on bundled armchair tubes [(n,n) tubes with $n = 10$–13] indicate a correlation between the pressure dependence of the tangential mode frequencies and the nanotube diameter. The same applies, however, to the radial mode, where such a correlation is not recognizable in the available experimental data.

Structural Transition at 2 GPa In their early work, Venkateswaran *et al.* [32] reported a sudden drop of the T mode intensity by a factor of 5 between 1.5 and 1.9 GPa and above 1.9 GPa a broadening of the T band with increasing pressure. The broadening turned out to be mostly reversible upon pressure release from the maximum value of 5.2 GPa. In contrast, only about half of the initial R and T band intensity was recovered, and the peak positions were shifted to slightly lower wavenumbers by 2–4 cm^{-1}. The observation that the pressure-induced changes were not fully reversible was taken as an indication that the intertubular contacts within the bundles might change under pressure.

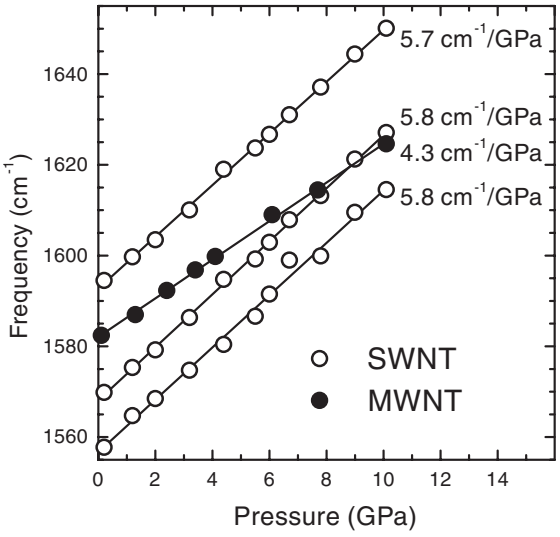

Figure 7: Wavenumbers vs pressure of the three T-band components of the AD-SWNTs shown in Fig. 6 and for the E_{2g}-like mode of AD multi-wall nanotubes. Reproduced from Ref. [36].

An abrupt decrease of the pressure dependences of the tangential mode wavenumbers was first reported by Peters *et al.* [34]. Figure 8 depicts the change in slope of the tangential modes of PLV-SWNTs at 1.7 GPa. Below the critical pressure, the modes shift at a rate of $\sim$10 cm^{-1}/GPa. Above 1.7 GPa, the slopes of the two higher-energy components reduce to $\sim$5.9 cm^{-1}/GPa and that of the lower-energy peak becomes as small as 0.7(1) cm^{-1}/GPa. The peak frequencies were observed to return to their initial values after pressure release, but only after some delay on the order of 30 minutes. These results motivated a reanalysis of the earlier data of Venkateswaran *et al.* [32] that had initially been represented by a quadratic polynomial. The reanalysis showed that the curvature of the tangential-band energy shift could possibly be interpreted as a change in slope of the wavenumber shift near 2 GPa [40]. The most intense component of the T-band then exhibits a shift of 7.5 cm^{-1}/GPa in the range 0–2 GPa and a smaller shift of 4.8 cm^{-1}/GPa in the range 2–5.5 GPa (Table 1). These observations were the first indications of a subtle structural transition in the nanotube bundles near 2 GPa that will be discussed in detail in section 3.3.

Shear Strain In two of the Raman studies on AD-SWNTs [43, 39], significant differences between the pressure shifts of the individual components were reported. Reich *et al.* [43] interpreted this finding in an experiment with excitation at 647 nm, i.e., where resonant Raman scattering mainly from metallic tubes is expected, in terms of shear strains due the difference in axial and radial compression, as discussed in the previous section. In armchair tubes, that are always metallic, this anisotropy is expected to result in different pressure derivatives for the frequency of modes with axial and circumferential displacement of the atoms [43]. Teredesai *et al.* [39], on the other hand, conducted the experiment with excitation at 515 nm, where semiconducting tubes should be in resonance. If a methanol/ethanol/water mixture was used as pressure medium, the three most intense components shifted at rates of 5.8–6.1 cm^{-1}/GPa, whereas two low-energy, low-intensity components of the T band shifted with 5.3 cm^{-1}/GPa (Fig. 9). This difference became much more pronounced, when water was used as pressure medium. In this case, wavenumber shifts in the range 3.7–8.0 cm^{-1}/GPa were observed. A possible cause for this change are nonhydrostatic stress components that may arise in water as a pressure medium that

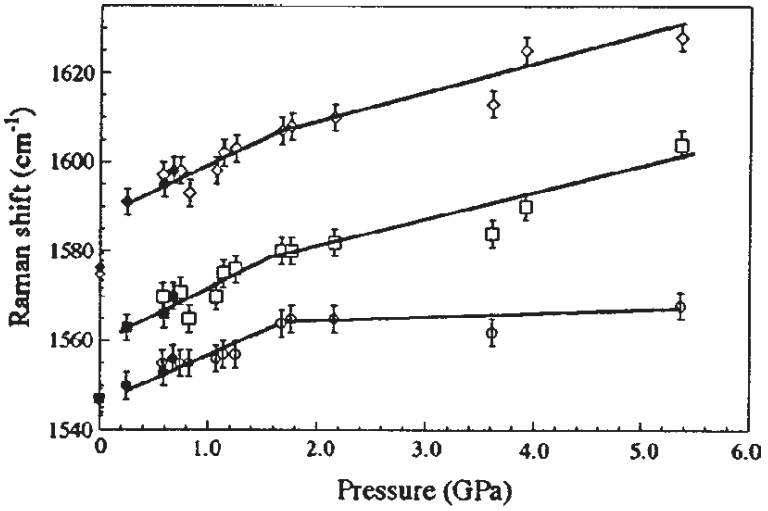

Figure 8: Raman shift vs pressure for tangential modes after Peters *et al.* [34]. The three tangential peaks are represented by circles, squares, and diamonds, respectively. Open (closed) symbols indicate data taken on pressure increase (decrease).

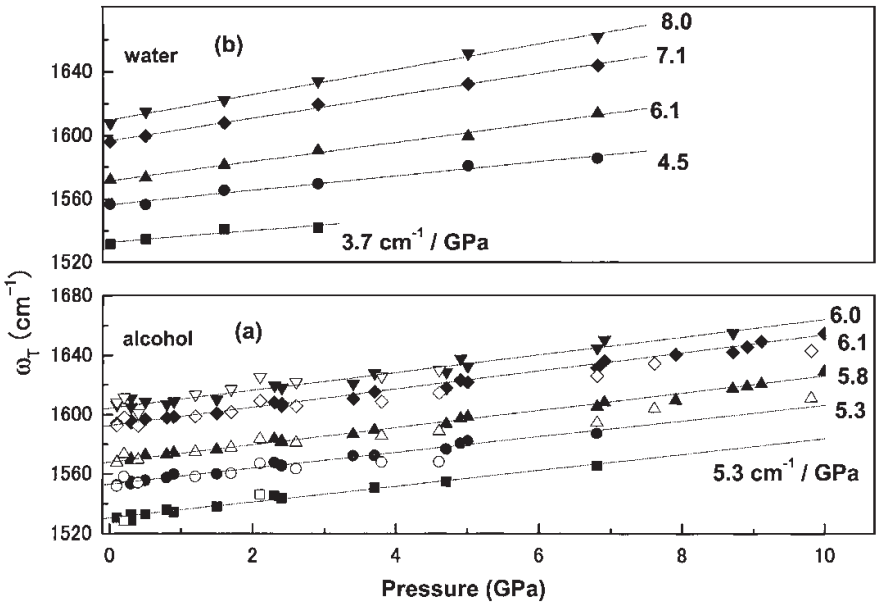

Figure 9: Variation of the tangential mode wavenumbers of AD bucky paper with respect to pressure, using (a) a 16:3:1 methanol/ethanol/water mixture and (b) pure water as pressure media. The solid (open) symbols represent data for increasing (decreasing) pressures. The straight lines are linear fits to the data with the resulting pressure derivatives (in cm^{-1}/GPa) given on the figure ($\lambda_{ex} = 515$ nm). Reproduced from Ref. [39].

solidifies at 1 GPa, whereas the alcohol mixture remains liquid up to 10 GPa.

Structural Resilience The structural stability of SWNTs under compression up to 30 GPa has been explored by Sood *et al.* [37, 38, 39]. Figure 10 depicts Raman spectra recorded on AD-SWNT bucky paper with a methanol/ethanol/water mixture as the pressure transmitting

medium. The signal intensity decreases continuously with increasing pressure up to 26 GPa. After pressure release, the initial Raman spectrum is essentially recovered. Compared to the initial spectrum, there is only an intensity loss of about 20% and a moderate increase in peak width. The peak positions as a function of pressure are shown in Fig. 11. The important result here is a pronounced softening that occurs for increasing pressures in the range of 10 to ∼16 GPa. Upon pressure decrease, essentially the same anomaly is observed. It should be mentioned that the anomaly may, in principle, be related to the solidification of the pressure transmitting medium at 10 GPa and the associated occurrence of shear strains above this pressure. Experiments with pressure media other than alcohol were, unfortunately, limited to maximum pressures of 9 GPa (nitrogen [33], solid at 2.5 GPa) and 7 GPa (water [39], solid at ∼1 GPa). Teredesai *et al.* [39] argued that the absence of a phase transition up to 6 GPa in the experiment with water would rule out the possibility that the 10-GPa anomaly could be related to the freezing of the pressure medium. For unambiguous evidence that the anomaly is an intrinsic property of carbon nanotubes, the softening should, ideally, be reproduced in an experiment to 15–20 GPa employing a fully hydrostatic pressure medium, i.e., helium.

In complementary x-ray diffraction work on the same type of sample by Sharma *et al.* [58], the (1 0) reflection of the two-dimensional triangular lattice of the SWNT bundles vanished at ∼10 GPa. They employed 4:1 methanol/ethanol as a pressure transmitter. A calculation of diffraction patterns showed that a hexagonal facetting of the nanotubes does not affect significantly the intensity of the (1 0) reflection. Altogether, the observations were interpreted in terms of a reversible loss of the translational coherence in the nanotube bundles. It is noteworthy that the (1 0) reflection was observed to vanish at a much lower pressure of ∼1.5 GPa in x-ray diffraction work by Tang *et al.* [59].

The combined Raman and x-ray diffraction results on the 10-GPa anomaly were interpreted in terms of a formation of kinks and fins as investigated in molecular dynamics simulations of highly strained nanotubes by Iijima *et al.* [60] and Yakobson *et al.* [61]. The formation of such distortions would explain the loss of translational coherence. Also, it would explain the apparent expansion of the triangular lattice that was observed for increasing pressure just before the disappearance of the (1 0) reflection [58]. The lattice expansion may then be the cause of the Raman mode softening. On the other hand, the axial strain of the nanotubes present at 10 GPa is much lower than that required to induce the kinks and fins in the molecular dynamics calculations. Whatever the structural changes may be, recovery of the initial Raman signature after pressure release evidences a remarkable resilience of SWNTs under high pressures.

3.3 Anomaly at 2 GPa

Summary of Experimental Indications In the preceding sections we have seen evidence of discontinuous changes in the Raman spectra of SWNTs near 2 GPa. In most experiments, the R band vanishes in the pressure range 1.5–3 GPa (Fig. 3). In one study [40], the radial mode could be followed up to 7 GPa, but it exhibited a substantial drop in intensity at about 2 GPa (Fig. 5). Peters *et al.* [34] and Venkateswaran *et al.* [40] reported a change in slope at 1.7 and 2 GPa, respectively, for the pressure-induced shift of the T band (Fig. 8). In contrast, Teredesai *et al.* [39] stated explicitly that they did not observe such change in slope. Finally, Venkateswaran *et al.* [32] and Obraztsova *et al.* [33] reported broadening of the tangential peaks to occur only for pressures above 2 GPa.

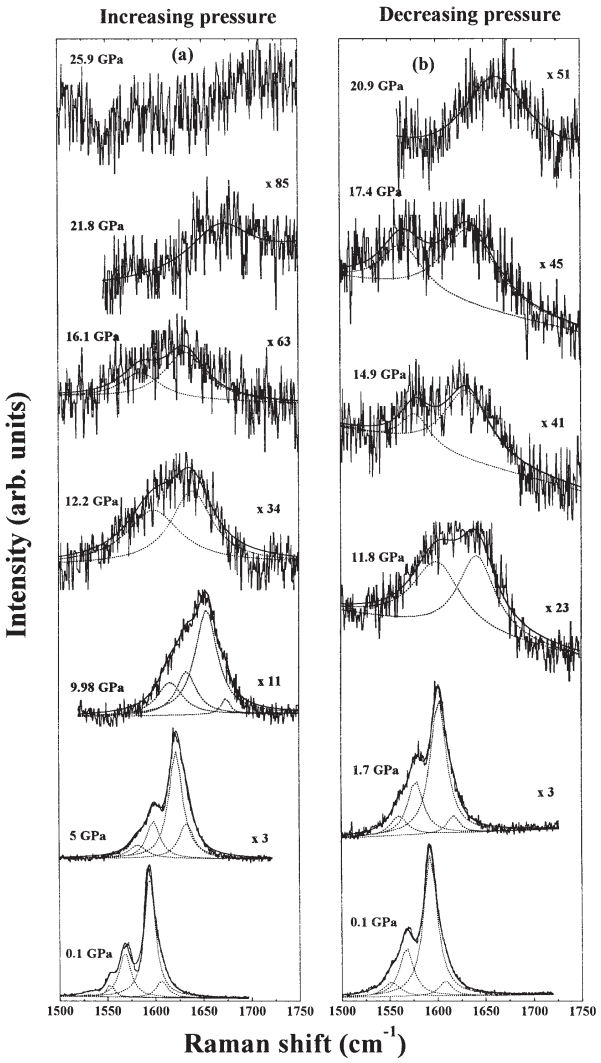

Figure 10: Raman spectra of AD-SWNT bucky paper in the tangential mode region for (a) increasing pressures to 26 GPa and (b) decreasing pressures (λ_{ex} = 515 nm). Dotted lines represent the decompositions into Lorentzian peaks fitted to the data. Reproduced from Ref. [38].

Theoretical Studies Molecular dynamics calculations (generalized tight-binding method) [32] of a $(9,9)$ nanotube bundle with triangular lattice evidenced a hexagonal distortion of the individual tubes. The facetting occurred already at zero calculated pressure, and it increased in magnitude with increasing pressure [Fig. 12(b)]. The lattice was allowed to adopt lower than hexagonal, i.e. oblique/monoclinic, symmetry. This resulted in a small difference between the two lattice parameters perpendicular to the nanotubes, which corresponds to an oval deformation of the tubes [Fig. 12(a)]. No structural transition was inferred from these calculations up to 5 GPa.

Calculations of a $(10,10)$ nanotube rope (universal force field method) gave rise to a rather different picture [34]. An important difference between a triangular lattice of $(9,9)$ and $(10,10)$ tubes is that the symmetry of the latter tubes is incompatible with the hexagonal lattice of the bundle. Consequently, already at zero pressure two different in-plane lattice constants were deduced, the tubes were ovally distorted, and the lattice of the nanotube bundle was monoclinic

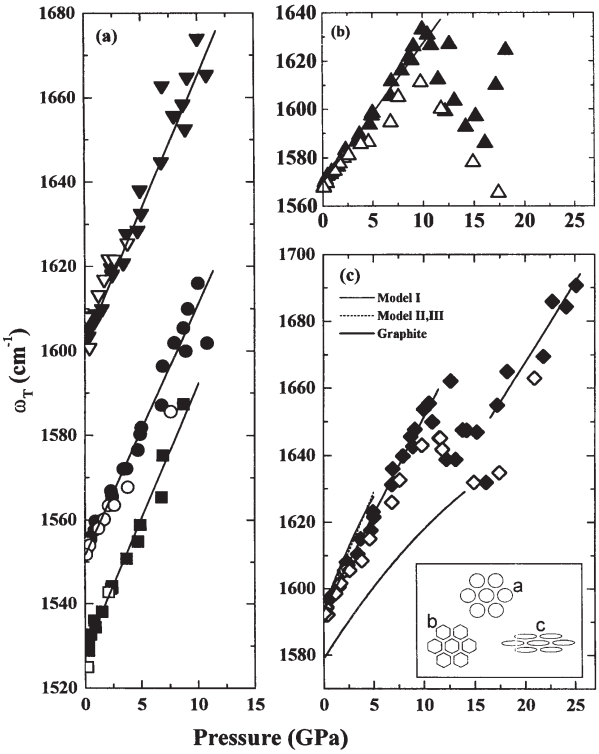

Figure 11: Peak positions as a function of pressure for the Raman spectra of AD-SWNT bucky paper shown in Fig. 10. Peak positions of (a) three components of the T band up to 10 GPa, of (b) the second-strongest component (1568-cm^{-1} at 0 GPa), and of (c) the most intense component (1594 cm^{-1} at 0 GPa). Solid (open) symbols represent data for increasing (decreasing) pressures. The straight lines at 0–10 GPa are linear fits to the data. Models I–III in panel (c) refer to the calculations of Venkateswaran *et al.* [32] in the range 0–5 GPa. Possible structural distortions of the nanotube cross section [57] are sketched in the inset. Reproduced from Ref. [38].

rather than hexagonal (Fig. 13). The calculated distortion increased continuously with increasing pressure up to 1.75 GPa, where a sudden transition to a more distorted structure occurred. This transition was associated with the experimentally observed change in shift rate of the tangential modes at 1.7 GPa [34] with the experimental and theoretical transition pressures being in remarkably good agreement. The oval distortion of the nanotubes would explain the disappearance of the radial band at about 2 GPa, because it is no longer an eigenmode.

A subsequent theoretical investigation [62] in the framework of density-functional theory (DFT) confirmed the different behavior for SWNTs whose symmetry is compatible or incompatible with a triangular lattice. For $(10, 10)$ nanotubes, a sudden transformation to an oval shape, accompanied by a transformation of the lattice from near-hexagonal to pronounced-monoclinic was predicted. If the generalized gradient approximation (GGA) to the DFT was employed, the transition pressure amounted to 2.5 GPa and the structure reverted to the near-hexagonal at 0.4 GPa upon pressure release. Using the local density approximation (LDA), a lower transition pressure of 1.2 GPa was calculated, and the monoclinic structure persisted down to ambient pressure upon unloading, i.e., the structure underwent an irreversible change. In contrast, for a bundle of $(12, 12)$ nanotubes a hexagonal deformation was inferred, and the lattice remained hexagonal over the whole pressure range of the calculation, 0–6 GPa.

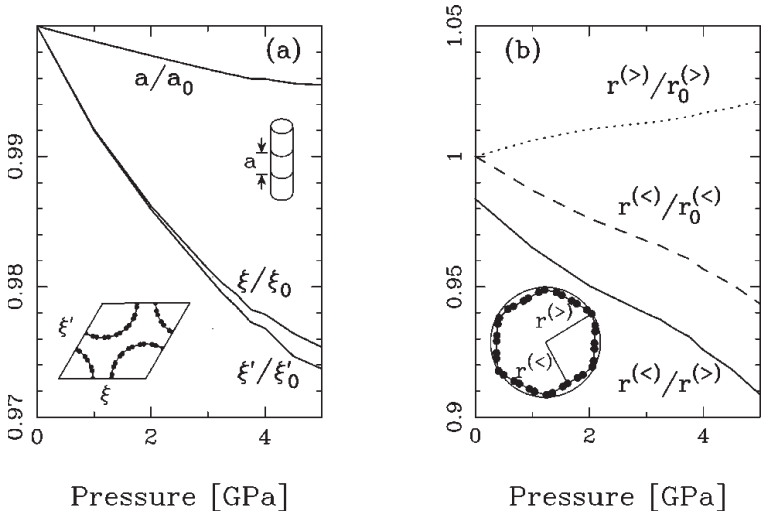

Figure 12: Pressure dependence, as calculated within model I of Ref. [32], of (a) the lattice constants and (b) the hexagonal distortion of the cross section of an individual $(9,9)$ nanotube in a bundle. The ratio $r^{(>)}/r^{(<)}$ serves as a measure of the distortion. For clarity the distortion depicted in the inset of (b) is exaggerated compared to the actual deformation at 5 GPa. Reproduced from Ref. [32].

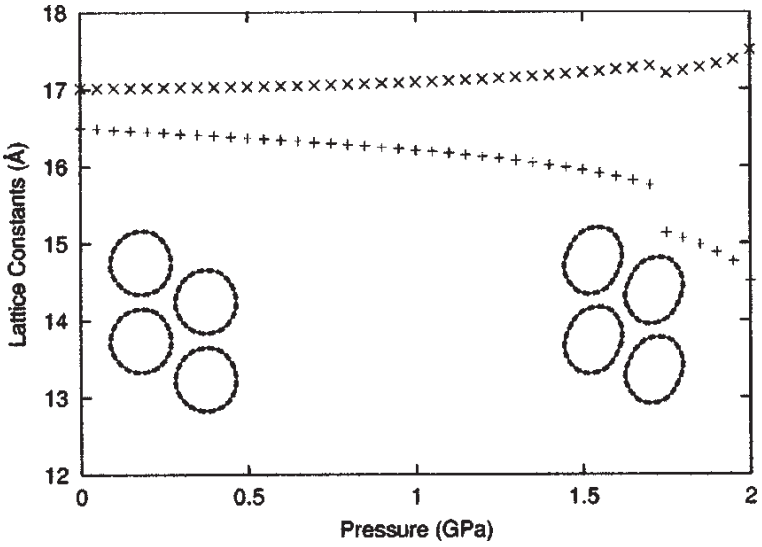

Figure 13: In-plane lattice constants vs pressure for a (10,10) nanorope. Insets: Cross sections of tubes at atmospheric pressure and 1.85 GPa. Reproduced from Ref. [34].

Structural Changes Contradicting conclusions were drawn from several diffraction experiments of SWNTs under pressure. As mentioned before, Tang *et al.* [59] reported the disappearance of the (1 0) reflection of the triangular lattice under hydrostatic conditions at 1.5 GPa (without, unfortunately, substantiating this claim by showing the corresponding diffractograms). At variance with this result, Sharma *et al.* [58] could follow the (1 0) reflection up to ∼10 GPa, and they did not find evidence for a structural transition at 1.7 GPa. The latter finding is in accordance with the fact that Teredesai *et al.* [39] did not observe, on the same type of sample, a change in wavenumber shift of the tangential modes near 1.7 GPa. Likewise, there is no consen-

sus on the question of reversibility of the structural changes. The results range from persistent deformations observed in high-resolution transmission electron microscopy (HRTEM) images after hydrostatic pressurization to only 1 GPa [41], over irreversible deterioration of the bundle structure after applying pressures of more than 4–5 GPa [59,63], to almost complete reversibility of the Raman spectrum of SWNTs even after subjecting them to a pressure of 30 GPa under nonhydrostatic conditions [39].

Conclusions Given the overall agreement on (i) the discontinuous reduction in intensity of Raman bands near 2 GPa and (ii) the theoretical results regarding the oval and hexagonal distortions of bundled nanotubes, one may interpret the 2-GPa anomaly as follows. In a typical carbon nanotube sample, a mixture of SWNTs is present with a range of diameters and chiralities. Part of them may have structures compatible with the triangular lattice, but for a substantial fraction this will not be the case. Quite likely, the *abrupt* intensity loss of the R band is therefore caused by an oval deformation of the nanotubes. If the nanotube sample contains a large fraction of tubes exhibiting the ovalization, it may also affect the tangential modes. Otherwise, the competition between hexagonal and oval distortion may mask or smear the change in slope so that it becomes difficult to detect. The *continuous* reduction in intensity may, at least in part, originate from the strengthened intertube interaction in the bundles under pressure. It quenches the nearly one-dimensional character of the electronic structure and should lead to a broadening of the sharp features in the electronic density of states and consequently reduce the resonant enhancement of the Raman signal.

The contradicting results compiled above may largely originate from differences in sample composition in terms of diameters and chiralities of the SWNTs. Variances in experimental conditions, in particular with regard to the laser excitation power, may also be of relevance. Substantial heating of carbon nanotubes due the incident laser radiation is known to occur already at moderate laser powers. For example, heating by several 100 K was reported for multiwall nanotubes with excitation powers of less than 4 mW and a laser spot diameter at the sample of 25 µm [64].

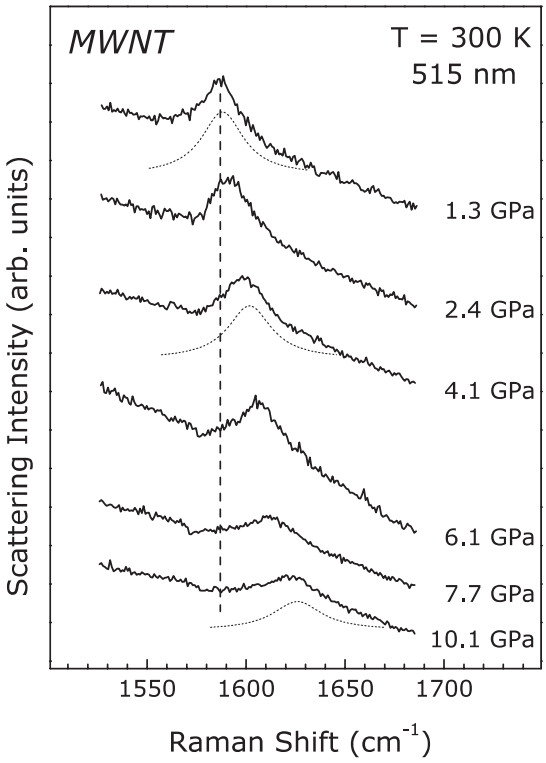

Figure 14: Raman spectra of the high-energy mode of multi-wall carbon nanotubes under hydrostatic pressure. Solid lines represent the experimental data, dashed lines depict Lorentzian peaks fitted to the spectra. Reproduced from Ref. [36].

4 Lattice Dynamics of MWNTs

Basic Results Raman spectra of arc-discharge-grown MWNTs under hydrostatic pressure up to 10 GPa (methanol/ethanol pressure medium) are depicted in Fig. 14. A single symmetric peak was resolved in the spectral region of the high-energy mode, corresponding to the in-plane $E_{2g}(2)$ phonons in graphite. With increasing pressure, it shifts towards higher wavenumbers at a rate of 4.3 cm^{-1}/GPa (Fig. 7). In a second study, MWNTs grown by chemical vapor deposition (CVD) were studied under pressure with both methanol/ethanol and condensed helium as a pressure medium. Essentially the same pressure coefficients were determined for the high-energy mode: 3.8(2) cm^{-1}/GPa and 3.7(1) cm^{-1}/GPa for the experiments with methanol/ethanol and He, respectively. The difference between the results of the two studies originates most likely from dissimilar tube dimensions (inner and outer diameters) in the AD- and the CVD-grown samples. The key result is that the pressure dependence of the high-energy mode in MWNTs is substantially smaller than in SWNTs (∼5–6 cm^{-1}/GPa, cf. Table 1) and even smaller than in graphite (4.7 cm^{-1}/GPa [25]).

Elasticity Theory The difference between the pressure coefficients of the high-energy modes in single- and multi-wall nanotubes was discussed in the framework of elasticity theory [36]. As mentioned above, this model approximates the nanotubes by a hollow cylinder with isotropic elastic properties within the sheet that is rolled up [54,36,55]. The axial strain u_{zz} of a closed hollow cylinder can be derived as $u_{zz} = -PA(1-2\nu)/E$, where ν denotes Poisson's ratio, E is

Young's modulus, and $A = R_o^2/(R_o^2 - R_i^2)$ is the ratio of total lid area to the area supported by the cylinder wall. R_i and R_o refer to the inner and outer diameters of the cylinder, respectively. On the assumption that the ratio ρ of the pressure coefficients of the high-energy modes in single- (SW) and multi-wall (MW) tubes equals the corresponding ratio of axial strain, Thomsen *et al.* [36] obtained

$$\rho = \frac{\mathrm{d}\ln\omega^{\mathrm{SW}}/\mathrm{d}P}{\mathrm{d}\ln\omega^{\mathrm{MW}}/\mathrm{d}P} = \frac{u_{zz}^{\mathrm{SW}}}{u_{zz}^{\mathrm{MW}}} = \frac{A^{\mathrm{SW}}}{A^{\mathrm{MW}}} \approx 1.5 \ , \tag{4}$$

where the inner and outer diameters of the SWNT were chosen as $R_i = 5.2$ Å, $R_o = 8.6$ Å (corresponding to a wall thickness of 3.4 Å), and for the MWNT the values $R_i = 20$ Å, $R_o = 75$ Å were used. The same result is obtained if one considers the ratio of circumferential strains. The result is in fair agreement with their experimental value of $\rho = 1.35$. The difference in pressure derivatives of the high-energy modes in single- and multi-wall nanotubes can thus be associated with the differences in wall thickness and tube diameter. The merit of this approach is not so much to make accurate quantitative predictions, but rather to help in the interpretation of experimental data in a relatively simple framework.

5 Structural Transformations of Carbon Nanotubes

Background The prospect of transforming graphite or other carbon-rich matter into diamond has fascinated researchers for a long time [65]. The most effective approach known to reach this goal is to subject the starting material (usually graphite) simultaneously to high pressures and high temperatures [65,66]. The addition of suitable catalysts can significantly reduce the pressure and/or temperature required to achieve the conversion. In recent years, carbon nanotubes have also been considered as a starting material for the diamond synthesis. It was argued that the curvature of the graphene sheets gives rise to a partial sp^3 hybridization that might result in a formation of covalent sp^3 C–C under milder (pressure and temperature) conditions [67]. Such expectations were promoted by the fact that various polymerized forms of the fullerene C_{60} can be obtained from a high-pressure/high-temperature treatment [68]. The possibility of pressure-induced structural transitions and polymerization of SWNTs was investigated theoretically [69, 70].

At ambient temperature and nearly hydrostatic conditions (He pressure medium), graphite is resistent to a transformation towards cubic diamond to at least 80 GPa [71]. Teredesai *et al.* [38] subjected SWNTs to 26 GPa under quasi-hydrostatic conditions (methanol/ethanol/water pressure medium) and found the observed changes to be almost fully reversible when comparing Raman spectra recorded at 0.1 GPa before and after the pressure cycle (Fig. 10). However, after removal of the pressure-cycled sample from the DAC and evaporation of the pressure medium, they did observe significant changes of the tangential and radial bands in the form of a peak down-shift by 6–10 cm^{-1} and some broadening (Fig. 15). On the basis of X-ray diffraction measurements on the recovered sample, the authors ruled out the possibility of graphitization since they did not observe an increase in intensity of the (0 0 2) reflection of graphite. Even for nonhydrostatic compression (without any pressure medium), changes to the Raman spectra of SWNTs were reported to be mostly reversible [39]. Obraztsova *et al.* [33] also reported some persistent broadening of the tangential band after subjecting PLV bucky paper to a maximum pressure of 8–9 GPa (nitrogen pressure medium). At variance with the previous authors, however, they did find evidence for the formation of graphitic needles at the bases of the SWNT bundles in HRTEM images (Fig. 16). There is a possibility that graphitic particles have also formed in the experiments of Teredesai *et al.* but remained undetected in the x-ray diffractograms due to a rather small particle size (x-ray reflection broadening due to size effects) and/or small volume fraction compared to the abundance of ∼8% graphite in the starting material [58].

Shear Deformation Intentional generation of shear strain in a modified DAC under load was reported to cause a conversion of graphite into amorphous carbon plus diamond particles (20–500 nm in diameter) at ambient temperature and pressures as low as 21–25 GPa [72]. In the spirit of this approach, Popov *et al.* [73] subjected PLV bucky paper to a shear deformation at high pressures. The shear forces were generated in a DAC by rotating one of the anvils around the axis of load, with the sample being pressurized without a pressure transmitting medium. Raman spectra were recorded both *in situ* to monitor the pressure-induced changes and on the recovered specimen in order to obtain information on irreversible structural changes (Fig. 17). Apart from some persistent broadening of the T-band, the main effect of the shear-deformation treatment appears to be a major reduction in intensity of all bands but the one near 1350 cm^{-1} (defect-related D-band). All bands, including the radial mode, remain observable, though. These

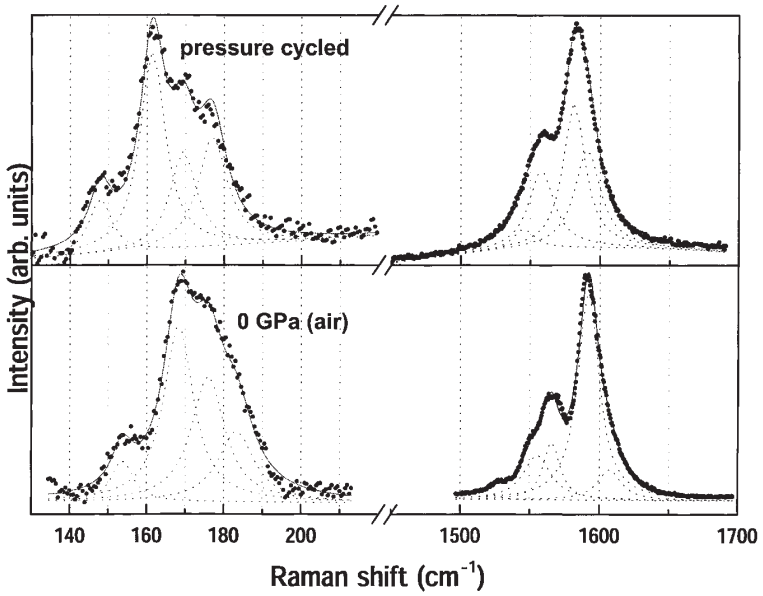

Figure 15: Raman spectra of AD-SWNTs as prepared and after pressure release from a maximum quasi-hydrostatic pressure of 26 GPa (methanol/ethanol/water pressure medium), showing changes of the R band and irreversible broadening of the T band. The measured spectra are represented by circles, solid lines are fits to the spectra with the dotted lines indicating the fitted Lorentzian peaks. Reproduced from Ref. [39].

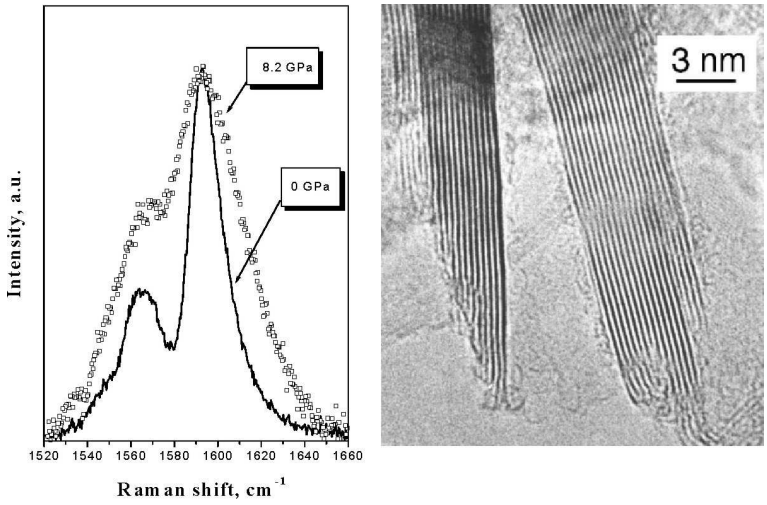

Figure 16: (left) Ambient-pressure Raman spectra of PLV bucky paper as prepared and after pressure release from a maximum quasi-hydrostatic pressure of 8.2 GPa (nitrogen pressure medium), showing irreversible broadening of the T band. (right) HRTEM image of graphitic needles that were observed at the base of SWNT bundles after application of hydrostatic pressure of 8–9 GPa. Reproduced from Ref. [33].

observation are consistent with expectations one may have on the basis of the irreversible changes reported in previous experiments, e.g., by Obraztsova *et al.* [33] and Teredesai *et al.* [39].

Popov *et al.* [73] identified the shear-deformation treated SWNTs as a "superhard" phase of SWNTs. Results of nano-indentation hardness measurements were presented, in the first place,

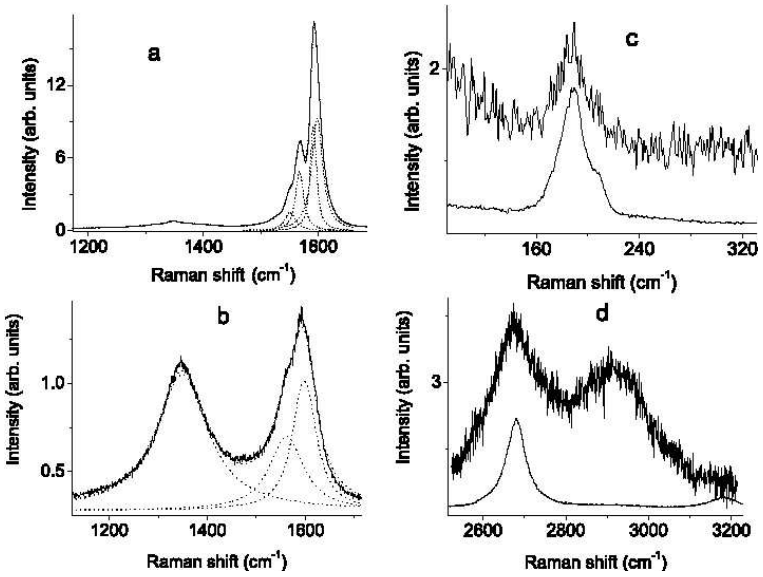

Figure 17: Ambient-pressure Raman spectra in the spectral region of the tangential modes ($\sim$1600 cm^{-1}) and the defect-related D band ($\sim$1350 cm^{-1}) of (a) SWNT as grown and (b) shear-deformation-treated SWNT after pressure release. (c) R bands and (d) second-order Raman spectra of as-grown SWNT (lower traces) and shear-deformation-treated SWNT (upper traces). Reproduced from Ref. [73].

in order to substantiate their claim. The recovered material is supposed to have a hardness in the range 62–150 GPa, i.e., in the hardness range spanned by cubic boron nitride and diamond. Hardness measurements with indentations as small as a few tens of nm appear to be a delicate procedure [74], the accuracy of which is difficult to assess. In the second place, they claim that the shear-deformation treated SWNT have a bulk modulus of 462–546 GPa, larger than that of diamond (442–446 GPa) [75, 76]. Besides the fact that a large bulk modulus is not a sufficient condition for high hardness [77], the claim turns out to be untenable in view of the available experimental data.

A crucial *assumption* in the determination of the bulk modulus (from the pressure dependence of the T band wavenumber) was that the mode Grüneisen parameter γ is about 1.0 for the T-like mode of the high-pressure treated SWNT. There is, however, no basis for such a supposition. Due to very anisotropic compression properties, the E_{2g}(-like) modes in graphite and as-grown SWNTs have mode Grüneisen parameters much smaller than 1, on the order of 0.1 [25]. Therefore, there is no reasonable *a priori* choice for the Grüneisen parameter, anything in the range 0.1–1 would be reasonable, and even values outside that range cannot be excluded. The assumption of $\gamma \approx 1$ does not appear suitable in order to substantiate the claim of a bulk modulus exceeding that of the most incompressible material known. So far, a shear-strain-induced transformation of SWNTs into a material with very high hardness has not been confirmed in independent investigations.

MWNT-to-Diamond Transformation Transformation of multi-wall nanotubes into diamond by simultaneous application of high pressures and high temperatures (HP/HT) was demonstrated by Tang *et al.* [78] and Yusa [79]. The former authors used purified MWNTs (and graphite for comparison) as a starting material together with a Ni-based alloy as a catalyst. The sample

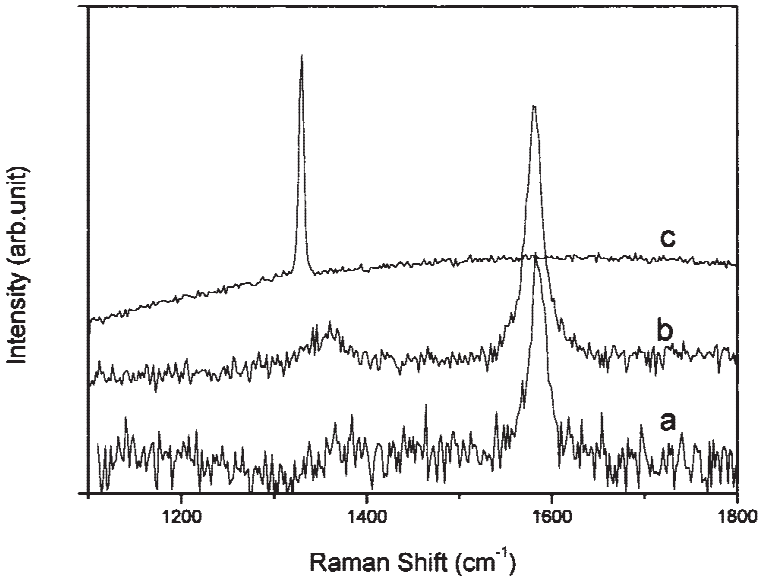

Figure 18: Raman spectra of (a) purified multi-wall carbon nanotubes as used as a starting material and after treatment at (b) 6.0 GPa/1600°C and (c) 7.0 GPa/1800°C. The material was purified again after the HP/HT treatment [80]. Reproduced from Ref. [78].

was pressurized in a boron nitride capsule using a 600-ton large-volume press. At pressures of 6.0 GPa and 7.0 GPa, the specimen were heated to 1600°C and 1800°C, respectively, for several seconds. The temperature was then decreased and the pressure released to ambient conditions in 1 min. The treatment at 6.0 GPa/1600°C had little effect on the Raman spectrum of the MWNTs (Fig. 18). After treatment at 7.0 GPa/1800°C and purification of the recovered material, however, the Raman spectrum changed completely. The T-band vanished and a new, relatively narrow peak appeared at 1332 cm^{-1}, which coincides with the position of the Raman peak of diamond. X-ray diffraction data were reported to support fully the notion of a transformation of the MWNTs into cubic diamond when subjected to 7.0 GPa and 1800°C [78]. Scanning electron microscopy (SEM) images of the transformed sample showed that there are many graphite-like flakes besides the diamond grains. The particles of unconverted carbon and the catalyst could be removed by etching with *aqua regia* (HCl and HNO_3). The SEM images indicated further that the diamond grains obtained from the nanotubes did not have a crystal form as well-shaped as those produced from graphite under the same pressure/temperature conditions. The former had many defects which appeared to be remnants of nanotubes. Tang *et al.* arrived at the conclusion that multi-wall carbon nanotubes are not a better source than graphite for the synthesis of diamond despite the partial sp^3-like hybridization.

The possibility of transforming MWNTs into diamond at high pressure in a laser-heated DAC *without* the use of a catalyst was investigated by Yusa [79], in continuation of previous experiments on graphite [81]. The starting nanotube sample (5 µm in thickness, 150 µm edge length) was enclosed in KBr to prevent direct thermal contact between the nanotubes and the diamond anvils. The nanotubes were heated with a continuous-wave CO_2 laser (maximum output power of 240 W) to a temperature of 2500–3000 K, as estimated from the emitted thermal radiation. After a few tens of seconds of heating, a transparent phase appeared at the irradiated spot. The transparent part of the recovered sample exhibited a single Raman peak at $\sim$1324 cm^{-1}, slightly

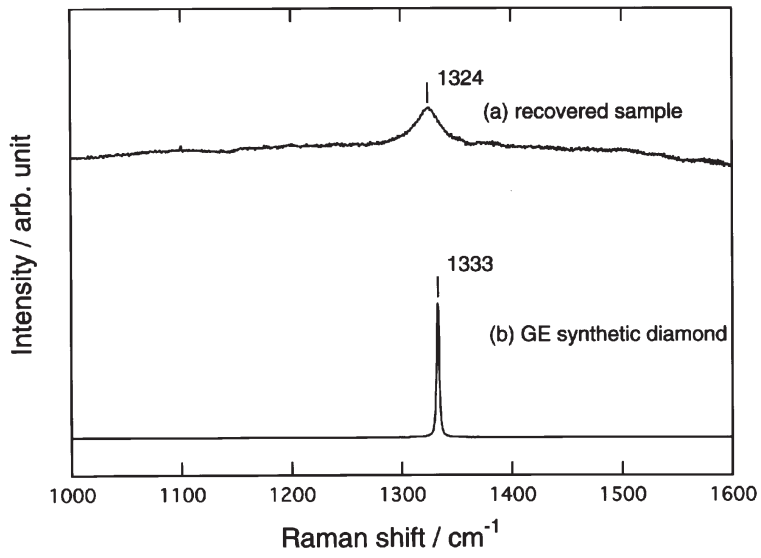

Figure 19: Raman spectra of (a) the transparent material produced from MWNTs at ∼17 GPa and laser-heating to 2500–3000 K in a DAC and (b) a synthetic diamond crystal. Reproduced from Ref. [79].

below the position of the Raman peak of bulk diamond (Fig. 19). Down-shift and broadening of the Raman peak were attributed to particle size effects [82]. The view that the MWNTs were converted to diamond was supported by electron diffraction on the recovered transparent material. It exhibited only the reflections of diamond, but not the characteristic (0 0 2) reflection of MWNTs and graphite. Further support came from electron energy loss spectroscopy (EELS, K-edge absorption and plasmon loss) that gave evidence for sp^3 hybridization and loss of the π-electron signature in the converted sample. EELS and energy-dispersive x-ray analysis (EDX) did not yield indication of the presence of any element other than carbon. SEM images evidenced a granular structure of the recovered material with particle sizes of less than 50 nm. The upper size limit was related to the diameter of the initial MWNTs and taken as indication that the nano-sized diamonds were formed by direct transformation of the nanotubes, without going through a molten state.

Yusa's observation of a granular structure is quite similar to the earlier findings of Tang *et al.* [78]. At variance with the latter authors, Yusa did not report the presence of graphitic particles. The assignment of the down-shift of the diamond Raman peak in one of the experiments to particle size effects may need reconsideration as the diamond grains appear to have a similar size distribution in both experiments.

Polymerization of SWNTs The possibility to polymerize single-wall carbon nanotubes at high pressures and temperatures was explored by Khabashesku *et al.* [67]. Purified PLV-grown SWNTs, pressed into pellets with a size of ∼2.5 mm, were used as the starting material. Pressures up to 10 GPa were generated in piston-cylinder-type and "toroid"-type high-pressure apparatuses. In several runs, samples were heated to temperatures in the range 200–1500°C for 5–300 s, quenched to ambient conditions, and then characterized by Raman spectroscopy, x-ray and electron diffraction, electron microscopy, EDX, and in some cases by electron microprobe analysis (EPMA).

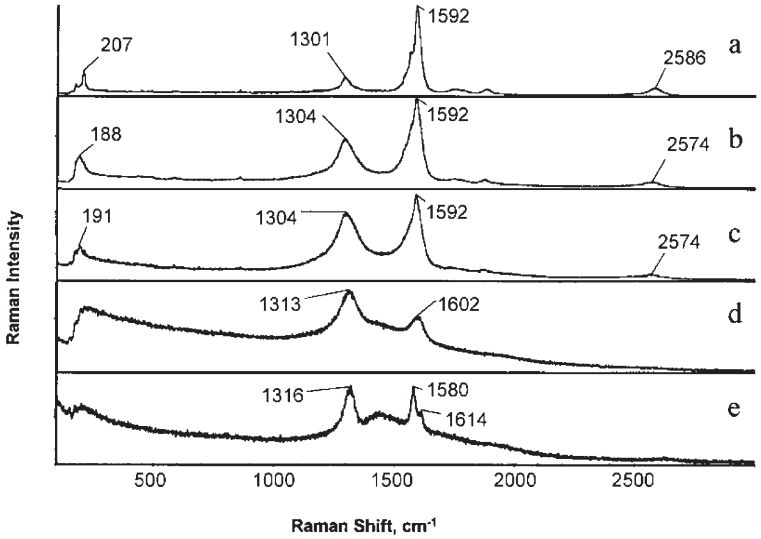

Figure 20: Raman spectra of SWNT samples after HP/HT-treatment at 8.0 GPa and temperatures of (a) 200°C, (b) 500°C, (c) 800°C, (d) 1200°C, and (e) 1500°C ($\lambda_{ex} = 780$ nm). Reproduced from Ref. [67].

The first set of experiments was performed at quite low a pressure of 1.5 GPa because of the structural changes occurring in SWNTs near 2 GPa (cf. section 3.3) and because C_{60} starts to polymerize at such low pressures [68]. Treatment at temperatures up to 700°C mostly affected the D mode near 1300 cm^{-1} in the Raman spectrum of the recovered material. This defect-related mode showed some increase in intensity with increasing maximum temperatures of 300, 500, and 700°C. The D mode was associated here with defects in the form of intertube sp^3-type C–C bonds on the basis of x-ray diffraction and SEM data. The initial SWNT bundles could mostly be restored after sonication of the HP/HT-treated material in propanol for two hours.

HP/HT treatment at 8.0 GPa and temperatures up to 1500°C lead to more pronounced changes. For temperatures of 1200 and 1500°C, the Raman R band near 200 cm^{-1} and the D band overtone near 2580 cm^{-1} disappeared, and the T band substantially decreased in intensity (Fig. 20). The intensity of the D band of all recovered samples was much larger than in the pristine SWNTs. With increasing temperature the D band shifted to higher wavenumbers. This was taken as indication of a possible formation of sp^3-type C–C bonds much like in diamond. Electron microscopy and electron diffraction indicated a polycrystalline structure of the samples. Treatment at the highest temperature of 1500°C, however, resulted in a predominant formation of graphite as evidenced by the Raman and x-ray diffraction data.

At a pressure of 9.5 GPa, polycrystalline material formed already at temperatures of 400 and 600°C. Electron diffraction data of the 600°C-sample was taken as evidence for the formation of particles of hexagonal and cubic diamond. Altogether, these experiments evidenced irreversible changes to SWNTs when subjected simultaneously to pressures up to 9.5 GPa and temperatures up to 1500°C. Changes to SWNT bundles subjected to 1.5 GPa could be reversed by sonication. SWNTs exposed to 9.5 GPa/600°C showed signs of a transformation into hexagonal and cubic diamond.

Conclusions A shear-deformation treatment of single-wall carbon nanotubes was reported to yield a "superhard" phase of carbon nanotubes. This claim, however, appears to require further experimental substantiation. SWNTs treated at high pressures/temperatures showed indication of the formation of covalent intertube C–C bonds, i.e., polymerization. At 9.5 GPa and 600°C, there were signs of a synthesis of hexagonal and cubic diamond particles. The transformation of multi-wall carbon nanotubes into diamond was achieved by simultaneous application of high pressures and temperatures. The results, however, fell short of the expectations that the conversion might be realized at milder pressure/temperature conditions than required for the transformation of graphite.

6 Concluding Remarks

Raman scattering studies of carbon nanotubes at high pressures have made important contributions to our understanding of these materials. In particular, they have pointed out the importance of the van-der-Waals type intertubule interaction, that had been assumed for a long time to have only negligible effect on the structural, vibrational, and electronic properties. There remain, however, a number of open questions and challenges. One of the latter is the investigation of truly individual SWNTs (rather than small bundles) under hydrostatic pressure. This would address the question of the effect of the van-der-Waals interaction in very small bundles raised by the investigation of solubilized SWNTs. Further progress in the preparation of debundled SWNTs may open way to such experiments. Alternatively, one may consider deposition and localization of individual nanotubes on the anvil of a DAC in the spirit of recent experiments [83] on isolated SWNTs at ambient conditions.

The interaction of pressure media with carbon nanotubes and possible intercalation has only been touched upon. It seems that methanol/ethanol does not enter the interstitial channels in SWNT bundles although geometrical constraints do not exclude this possibility [32]. Helium and nitrogen were employed as pressure media in a few cases [33,40], but without obvious effect on the nanotube properties. On the other hand, the condensation of He in the inside and the interstitial channels of SWNTs was studied theoretically [84,85]. Helium was predicted to form a one-dimensional liquid or solid within the tubes/channels. Intercalation of He or other small atoms/molecules into carbon nanotubes at high pressure may provide a means to realize and study quasi-one-dimensional liquids.

Raman spectroscopy has proven a useful tool to monitor attempts to transform carbon nanotubes into diamond and other "superhard" materials. Both single- and multi-wall carbon nanotubes were reported to transform into diamond at simultaneously high pressures and temperatures. So far, however, the results fell short of the expectations that this transformation may occur at milder conditions than in the case of graphite. Along this line of thought, one may speculate about the possibility of reacting carbon nanotubes with nitrogen in a laser-heated DAC in order to synthesize carbon nitride phases. This class of compounds has attracted a lot of interest in recent years [77,86,87] because of predictions of a high bulk modulus of β-C_3N_4 comparable to that of diamond [88]. The calculated shear modulus, however, amounted only to $\sim$60% of that of diamond so that one should expect a hardness closer to that of cubic boron nitride. Other carbon nitride phases such as spinel-type C_3N_4 [86] may, however, possess a much higher hardness. The prospect of possibly synthesizing new carbon phases and substances of high hardness will probably stimulate further research on the pressure-induced structural transformations of carbon nanotubes.

7 Acknowledgements

I would like to thank U. Venkateswaran, A. K. Sood, U. Schlecht, and K. Syassen for stimulating and helpful discussions. In addition, I acknowledge fruitful collaboration with H. Jantoljak, C. Thomsen, U. Venkateswaran, G. Duesberg, L. Farina, and K. Syassen in a number studies, part of which have been mentioned in this work.

References

[1] P. M. Ajayan and O. Z. Zhou, in *Carbon Nanotubes*, Vol. 80 of *Topics in Applied Physics*, edited by M. S. Dresselhaus, G. Dresselhaus, and P. Avouris (Springer-Verlag, Berlin, 2001), pp. 391–425.

[2] S. S. Fan, M. G. Chapline, N. R. Franklin, T. W. Tombler, A. M. Cassell, and H. J. Dai, Science **283**, 512 (1999).

[3] Q. H. Wang, A. A. Setlur, J. M. Lauerhaas, J. Y. Dai, E. W. Seelig, and R. P. H. Chang, Appl. Phys. Lett. **72**, 2912 (1998).

[4] W. B. Choi, D. S. Chung, J. H. Kang, H. Y. Kim, Y. W. Jin, I. T. Han, Y. H. Lee, J. E. Jung, N. S. Lee, G. S. Park, and J. M. Kim, Appl. Phys. Lett. **75**, 3129 (1999).

[5] C. Liu, Y. Y. Fan, M. Liu, H. T. Cong, H. M. Cheng, and M. S. Dresselhaus, Science **286**, 1127 (1999).

[6] S. J. Tans, A. R. M. Verschueren, and C. Dekker, Nature **393**, 49 (1998).

[7] J. Kong, N. R. Franklin, C. W. Zhou, M. G. Chapline, S. Peng, K. J. Cho, and H. J. Dai, Science **287**, 622 (2000).

[8] P. Kim and C. M. Lieber, Science **286**, 2148 (1999).

[9] S. Iijima and T. Ichihashi, Nature **363**, 603 (1993).

[10] D. S. Bethune, C. H. Kiang, M. S. de Vries, G. Gorman, R. Savoy, J. Vazquez, and R. Beyers, Nature **363**, 605 (1993).

[11] S. Iijima, Nature **354**, 56 (1991).

[12] M. Dresselhaus, G. Dresselhaus, and P. Eklund, *Science of Fullerenes and Carbon Nanotubes* (Academic Press, New York, 1996).

[13] R. Saito, G. Dresselhaus, and M. S. Dresselhaus, *Physical Properties of Carbon Nanotubes* (Imperial College Press, London, 1998).

[14] *Carbon Nanotubes*, Vol. 80 of *Topics in Applied Physics*, edited by M. S. Dresselhaus, G. Dresselhaus, and P. Avouris (Springer-Verlag, Berlin, 2001).

[15] M. S. Dresselhaus and P. C. Eklund, Adv. Phys. **49**, 705 (2000).

[16] H. Dai, in *Carbon Nanotubes*, Vol. 80 of *Topics in Applied Physics*, edited by M. S. Dresselhaus, G. Dresselhaus, and P. Avouris (Springer-Verlag, Berlin, 2001), pp. 29–53.

[17] A. Thess, R. Lee, P. Nikolaev, H. Dai, P. Petit, J. Robert, C. Xu, Y. H. Lee, S. G. Kim, A. G. Rinzler, D. T. Colbert, G. E. Scuseria, D. Tománek, J. E. Fischer, and R. E. Smalley, Science **273**, 483 (1996).

[18] A. Krishnan, E. Dujardin, T. W. Ebbesen, P. N. Yianilos, and M. M. J. Treacy, Phys. Rev. B **58**, 14013 (1998).

[19] P. Poncharal, Z. L. Wang, D. Ugarte, and W. A. de Heer, Science **283**, 1513 (1999).

[20] B. I. Yakobson and P. Avouris, in *Carbon Nanotubes*, Vol. 80 of *Topics Appl. Phys.*, edited by M. S. Dresselhaus, G. Dresselhaus, and P. Avouris (Springer-Verlag, Berlin, 2001), pp. 287–329.

[21] A. M. Rao, E. Richter, S. Bandow, B. Chase, P. C. Eklund, K. A. Williams, S. Fang, K. R. Subbaswamy, M. Menon, A. Thess, R. E. Smalley, G. Dresselhaus, and M. S. Dresselhaus, Science **275**, 187 (1997).

[22] S. Bandow, S. Asaka, Y. Saito, A. M. Rao, L. Grigorian, E. Richter, and P. C. Eklund, Phys. Rev. Lett. **80**, 3779 (1998).

[23] M. S. Dresselhaus and G. Dresselhaus, in *Light Scattering in Solids III*, Vol. 51 of *Topics in Applied Physics*, edited by M. Cardona and G. Güntherodt (Springer Verlag, Berlin, 1982), pp. 3–57.

[24] F. Tuinstra and J. L. Koenig, J. Chem. Phys. **53**, 1126 (1970).

[25] M. Hanfland, H. Beister, and K. Syassen, Phys. Rev. B **39**, 12598 (1989).

[26] I. Pócsik, M. Hundhausen, M. Koós, and L. Ley, J. Non.-Cryst. Solids **227–230**, 1083 (1998).

[27] R. J. Nemanich and S. A. Solin, Phys. Rev. B **20**, 392 (1979).

[28] T. W. Ebbesen and P. M. Ajayan, Nature **358**, 220 (1992).

[29] C. Journet, W. K. Maser, P. Bernier, A. Loiseau, M. L. delaChapelle, S. Lefrant, P. Deniard, R. Lee, and J. E. Fischer, Nature **388**, 756 (1997).

[30] J. Liu, A. G. Rinzler, H. Dai, J. H. Hafner, R. K. Bradley, P. J. Boul, A. Lu, T. Iverson, K. Shelimov, C. B. Huffman, F. Rodriguez-Macias, Y.-S. Shon, T. R. Lee, D. T. Colbert, and R. E. Smalley, Science **280**, 1253 (1998).

[31] H. Dai, J. Kong, C. Zhou, N. Franklin, T. Tombler, A. Cassell, S. Fan, and M. Chapline, J. Phys. Chem. B **103**, 11246 (1999).

[32] U. D. Venkateswaran, A. M. Rao, E. Richter, M. Menon, A. Rinzler, R. E. Smalley, and P. C. Eklund, Phys. Rev. B **59**, 10928 (1999).

[33] E. D. Obraztsova, H. T. Lotz, J. A. Schouten, M. E. Kooi, A. V. Osadchy, V. L. Kuznetsov, and V. I. Zaikovskii, in *Electronic properties of novel materials – science and technology of molecular nanostructures*, Vol. 486 of *AIP Conference Proceedings*, edited by H. Kuzmany (American Institute of Physics, Melville, 1999), pp. 333–337.

[34] M. J. Peters, L. E. McNeil, J. P. Lu, and D. Kahn, Phys. Rev. B **61**, 5939 (2000).

[35] C. Thomsen, S. Reich, A. R. Goñi, H. Jantoljak, P. M. Rafailov, I. Loa, K. Syassen, C. Journet, and P. Bernier, phys. stat. sol. (b) **215**, 435 (1999).

[36] C. Thomsen, S. Reich, H. Jantoljak, I. Loa, K. Syassen, M. Burghard, G. S. Duesberg, and S. Roth, Appl. Phys. A **69**, 309 (1999).

[37] A. K. Sood, P. V. Teresdesai, D. V. S. Muthu, R. Sen, A. Govindaraj, and C. N. R. Rao, phys. stat. sol. (b) **215**, 393 (1999).

[38] P. V. Teredesai, A. K. Sood, D. V. S. Muthu, R. Sen, A. Govindaraj, and C. N. R. Rao, Chem. Phys. Lett. **319**, 296 (2000).

[39] P. V. Teredesai, A. K. Sood, S. M. Sharma, S. Karmakar, S. K. Sikka, A. Govindaraj, and C. N. R. Rao, phys. stat. sol. (b) **223**, 479 (2001).

[40] U. D. Venkateswaran, E. A. Brandsen, U. Schlecht, A. M. Rao, E. Richter, I. Loa, K. Syassen, and P. C. Eklund, phys. stat. sol. (b) **223**, 225 (2001).

[41] E. D. Obraztsova, in *Frontiers of High Pressure Research II: Application of High Pressure to Low-Dimensional Novel Electronic Materials*, Vol. 48 of *NATO SCIENCE SERIES: II: Mathematics, Physics and Chemistry*, edited by H. D. Hochheimer, B. Kuchta, P. K. Dorhout, and J. L. Yarger (Kluwer Academic Publishers, Dordrecht, 2001), pp. 473–482.

[42] U. Schlecht, U. D. Venkateswaran, E. Richter, J. Chen, R. C. Haddon, P. C. Eklund, and A. M. Rao, preprint (unpublished).

[43] S. Reich, H. Jantoljak, and C. Thomsen, Phys. Rev. B **61**, 13389 (2000).

[44] D. Kahn and J. P. Lu, Phys. Rev. B **60**, 6535 (1999).

[45] M. Menon, E. Richter, and K. R. Subbaswamy, J. Chem. Phys. **104**, 5875 (1996).

[46] L. Henrard, E. Hernández, P. Bernier, and A. Rubio, Phys. Rev. B **60**, R8521 (1999).

[47] L. Henrard, V. N. Popov, and A. Rubio, Phys. Rev. B **64**, 205403 (2001).

[48] J. Kürti, G. Kresse, and H. Kuzmany, Phys. Rev. B **58**, R8869 (1998).

[49] A. M. Rao, J. Chen, E. Richter, U. Schlecht, P. C. Eklund, R. C. Haddon, U. D. Venkateswaran, Y.-K. Kwon, and D. Tománek, Phys. Rev. Lett. **86**, 3895 (2001).

[50] J. Chen, M. A. Hamon, H. Hu, Y. Chen, A. M. Rao, P. C. Eklund, and R. C. Haddon, Science **282**, 95 (1998).

[51] J. Chen, A. M. Rao, S. Lyuksyutov, M. E. Itkis, M. A. Hamon, H. Hu, R. W. Cohn, P. C. Eklund, D. T. Colbert, R. E. Smalley, and R. C. Haddon, J. Phys. Chem. B **105**, 2525 (2001).

[52] E. Richter and K. R. Subbaswamy, Phys. Rev. Lett. **79**, 2738 (1997).

[53] M. Milnera, J. Kürti, M. Hulman, and H. Kuzmany, Phys. Rev. Lett. **84**, 1324 (2000).

[54] G. G. Tibbetts, J. Cryst. Growth **66**, 632 (1984).

[55] S. Reich, C. Thomsen, and P. Ordejón, Phys. Rev. B **65**, 153407 (2002).

[56] B. Alzyab, C. H. Perry, C. Zahopoulos, O. A. Pringle, and R. M. Nicklow, Phys. Rev. B **38**, 1544 (1988).

[57] S. A. Chesnokov, V. A. Nalimova, A. G. Rinzler, R. E. Smalley, and J. E. Fischer, Phys. Rev. Lett. **82**, 343 (1999).

[58] S. M. Sharma, S. Karmakar, S. K. Sikka, P. V. Teredesai, A. K. Sood, A. Govindaraj, and C. N. R. Rao, Phys. Rev. B **63**, 205417 (2001).

[59] J. Tang, L.-C. Qin, T. Sasaki, M. Yudasaka, A. Matsushita, and S. Iijima, Phys. Rev. Lett. **85**, 1887 (2000).

[60] S. Iijima, C. Brabec, A. Maiti, and J. Bernholc, J. Chem. Phys. **104**, 2089 (1996).

[61] B. I. Yakobson, C. J. Brabec, and J. Bernholc, Phys. Rev. Lett. **76**, 2511 (1996).

[62] M. H. F. Sluiter, V. Kumar, and Y. Kawazoe, Phys. Rev. B **65**, 161402 (2002).

[63] S. Rols, I. N. Goncharenko, R. Almairac, J. L. Sauvajol, and I. Mirebeau, Phys. Rev. B **64**, 153401 (2001).

[64] F. Huang, K. T. Yue, P. Tan, S.-L. Zhang, Z. Shi, X. Zhou, and Z. Gu, J. Appl. Phys. **84**, 4022 (1998).

[65] R. M. Hazen, *The diamond makers* (Cambridge University Press, Cambridge, 1999).

[66] E. Yu. Tonkov, in *High Pressure Phase Transformations* (Gordon and Breach, Philadelphia, 1992), Vol. 1, pp. 141–143.

[67] V. N. Khabashesku, Z. Gu, B. Brinson, J. L. Zimmerman, J. L. Margrave, V. A. Davydov, L. S. Kashevarova, and A. V. Rakhmanina, J. Phys. Chem. B **106**, 11155 (2002).

[68] B. Sunqvist, Adv. Phys. **48**, 1 (1999).

[69] L. A. Chernozatonskii, Chem. Phys. Lett. **297**, 257 (1998).

[70] T. Yildirim, O. Gülseren, Ç. Kılıç, and S. Ciraci, Phys. Rev. B **62**, 12648 (2000).

[71] A. F. Goncharov, Sov. Phys. JETP **71**, 1025 (1990), [Zh. Eksp. Teor. Fiz. **98**, 1824 (1990)].

[72] V. V. Aksenenkov, V. D. Blank, N. F. Borovikov, V. G. Danilov, and K. I. Kozorezov, Phys. Dokl. **39**, 700 (1994), [Doklady Akademii Nauk **338**, 472 (1994)].

[73] M. Popov, M. Kyotani, R. J. Nemanich, and Y. Koga, Phys. Rev. B **65**, 33408 (2002).

[74] A. Richter, R. Ries, R. Smith, M. Henkel, and B. Wolf, Diamond Relat. Mater. **9**, 170 (2000), and references therein.

[75] H. J. McSkimin, P. Andreatch, Jr., and P. Glynn, J. Appl. Phys. **43**, 985 (1972).

[76] I. D. Ph. Gillet, G. Fiquet, B. Reynard, and M. Hanfland, Phys. Rev. B **60**, 14660 (1999).

[77] J. Haines, J. Léger, and G. Bocquillon, Annu. Rev. Mater. Res. **31**, 1 (2001).

[78] D. S. Tang, L. C. Chen, L. J. Wang, L. F. Sun, Z. Q. Liu, G. Wang, W. Y. Zhou, and S. S. Xie, J. Mater. Res. **15**, 560 (2000).

[79] H. Yusa, Diamond Relat. Mater. **11**, 87 (2002).

[80] S. S. Xie, private communication (2003).

[81] H. Yusa, K. Takemura, Y. Matsui, H. Morishima, K. Watanabe, H. Yamawaki, and K. Aoki, Appl. Phys. Lett. **72**, 1843 (1998).

[82] M. Yoshikawa, Y. Mori, M. Maegawa, G. Katagiri, H. Ishida, and A. Ishitani, Appl. Phys. Lett. **62**, 3114 (1993).

[83] G. S. Duesberg, I. Loa, M. Burghard, K. Syassen, and S. Roth, Phys. Rev. Lett. **85**, 5436 (2000).

[84] M. C. Gordillo, J. Boronat, and J. Casulleras, Phys. Rev. B **61**, R878 (2000).

[85] M. W. Cole, V. H. Crespi, G. Stan, C. Ebner, J. M. Hartman, S. Moroni, and M. Boninsegni, Phys. Rev. Lett. **84**, 3883 (2000).

[86] T. Malkow, Mater. Sci. Eng. **A292**, 112 (2000).

[87] E. G. Wang, Prog. Mater. Sci. **41**, 241 (1997).

[88] D. M. Teter and R. J. Hemley, Science **271**, 53 (1996).